Electromagnetic and Mechanical Design of a Hermetically Sealed Magnetic Gear for a Marine Hydrokinetic Generator

Hossein Baninajar, Jonathan Z. Bird
Portland State University
Portland, OR, USA
hossein@pdx.edu , bird@pdx.edu

Sina Modaresahmadi, Wesley Williams
University of North Carolina at Charlotte
Charlotte, NC, USA
smodares@uncc.edu, wbwillia@uncc.edu

***Abstract*— This paper presents a new type of hermetically sealed magnetically geared generator typology for a marine hydrokinetic application. The proposed magnetically geared generator is composed of two series connected magnetic gearbox stages with the second stage having an integrated stator. This paper focuses only on presenting the electromagnetic design for the first stage magnetic gearbox with a 5kW (at 40RPM) rating. A volumetric and mass torque density trade-off analysis is utilized in order to arrive at a high torque density design. The designed magnetic gearbox uses a unique laminated flux concentration inner rotor and Halbach array outer rotor typology with a 6.67:1 gear ratio. A mechanical deflection analysis is performed to verify that the proposed magnetic gearbox is mechanically robust.**

Keywords—Magnetic gear, Halbach array, marine hydrokinetic energy, finite element analysis

I. Introduction

The design of a rotary based marine hydrokinetic (MHK) generator is extremely challenging because the rotary speeds created by the ocean are very low, typically less than 40 RPM, and the torque is extremely high. Due to its high torque density a mechanical gearbox is often considered for use in a MHK generator [1]. Currently, such a conversion approach is used in the majority of high-power wind turbines. Unfortunately, wind turbine gearboxes have been one of the main causes of wind turbine down-time [2] and therefore it is likely that a mechanical gearbox, used in a MHK generator, would also suffer from the same long-term reliability issues.

The main alternative to the mechanical gearbox is the direct-drive (DD) PM generator [1]. The use of the DD-PM generator removes the mechanical gearbox reliability concerns. However, the torque density of a DD-PM generator is thermally limited (by current) and so a PM generator does not normally operate at a magnetic shear stress above 20-40kN/m^2 [3]. Therefore, the torque densities is normally not greater than 50N·m/L [4] during continuous operation. For this reason, DD-PM generators become very large when scaled-up in size. This large size makes them difficult to integrate within the MHK structure and it also limits the DD-PMs scalability. It also makes the initial cost of the DD-PM uncompetitive when compared with a mechanically geared generator. In order to try to make MHK generators more reliable, and therefore reduce the levelized cost of energy, a number of authors have recently proposed using magnetic gearing technology [5-8] this paper investigates the performance capabilities of a new type of hermetically sealed rotary magnetic gearbox (MG).

II. A Coaxial Magnetic Gearbox

A coaxial MG uses a contactless mechanism for speed amplification [9]. An example of a surface mounted coaxial MG design is shown in Fig. 1. There is an inner rotor, consisting of p_1 pole-pair rotating at ω_1, a middle rotor with n_2 ferromagnetic slots that rotates at ω_2 and an outer rotor with p_3 pole-pair that can rotate at ω_3. In order to create field coupling and maximize torque the following condition must be met

$$n_2 = p_1 + p_3 \tag{1}$$

The rotational speed relationship between the rotors is then

$$\omega_1 = (1 + G_r)\omega_2 - G_r\omega_3 \tag{2}$$

where G_r is the gear ratio

$$G_r = \frac{p_3}{p_1} \tag{3}$$

If ω_3 = 0 the torque density is maximized, and a fixed gear ratio is achieved.

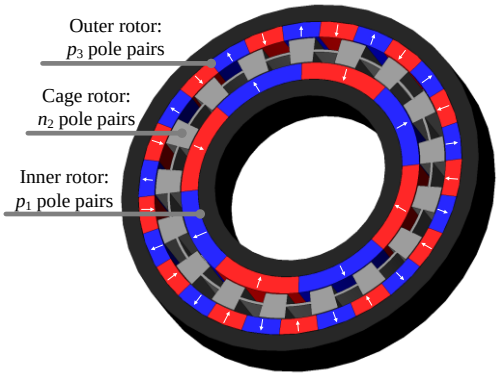

Fig. 1. A coaxial MG using surface PMs. p_1=4 pole-pairs, n_2=17 steel poles and p_3=13 pole-pairs on outer rotor.

Along with not needing gear lubrication and offering the ability to potentially increase efficiency a MG has unique features such as inherent overload protection, since if excessive torque is applied to a MG the rotors will slip poles, in contrast, a mechanical gearbox would catastrophically fail. This therefore changes the sizing requirement, and control approach, needed when using a MG within a MHK power-take-off. Also, the losses within a MG are primarily frequency dependent and therefore in low speed applications this can be an advantage.

By integrating a stator winding within the MG a magnetically geared generator (MGG) can be created. MGGs with torque densities up to 100N·m/L have recently been experimentally demonstrated [11]. However, only a few MGG have so far been built [5, 11, 12] and their ultimate performance capabilities are still not well understood. Recently a MHK MGG was design and experimentally tested in [5]. However, the operating gear ratio was insufficiently high for many MHK devices. In this paper a new type of multistage MHK generator is proposed that uses a unique hermetically sealed design. An overview of the design is illustrated in Fig. 2. The MHK generator is made up of two series connected MG stages. The first stage has a fixed modulator section ($\omega_2 = 0$) this then enables the generator to be hermetically sealed.

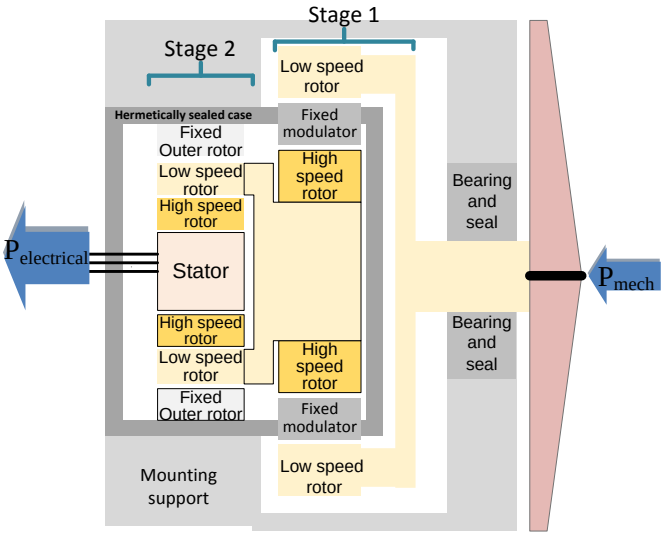

Fig. 2. Sketch illustrating an approach to designing a hermetically sealed magnetically geared marine hydrokinetic generator (Sizing not to scale)

III. Magnetic Gearbox Analysis

This paper will focus on presenting the electromagnetic design of the stage 1 section of a 5kW (at 40RPM) MHK generator. The required design requirement for the stage 1 MG are given in Table 1. The stage 1 MG central cage rotor is held fixed $\omega_2 = 0$, this makes achieving the required high torque density more challenging as the cage rotor experiences the highest torque.

A. Flux Concentration Typology

Initially a flux concentrator rotor typology [13, 14] was considered as it was shown to be able to achieve a relatively high torque density. The design geometry for a segment of the flux concentration MG typology is shown in Fig. 3. The chosen pole combination is $(p_1,n_2,p_3) = (6,46,40)$. Using this pole combination, the gear ratio is $G_r = 40/6 = 6.6\dot{7}$. It can be noted that this (6,46,40) pole combination is devisable by 2. This thereby provides symmetry and enables the MG to be simulated using an 180° model. This greatly reduces the transient loss calculation time. The pole values are based off of a $(p_1,n_2,p_3) = (3,23,20)$ combination. As both 3 and 23 are prime numbers this results in a low torque ripple design. Only odd harmonics are created by the flux concentration rotors and therefore the fact that all pole combinations are divisible by 2 does not affect the torque ripple. The central fixed cage rotor was chosen to have an even number of segments, $n_2 = 46$, and this therefore helps create a more even radial force distribution.

The MG design utilizes a laminated structure and also uses a unique mechanical construction approach. The outer rotor is supported mechanically by the outer non-magnetic (316 grade steel) rods. The central rotor is supported using non-magnetic rectangular support rods and the inner rotor is supported by one outer magnetic rod (1045 grade steel) and an inner non-magnetic rod (316 grade steel). The laminations are made of M-19 and the magnet type is N-48H. The outer and central laminations are made of one contiguous lamination piece. While the inner rotor is made up of 12 individual lamination segments. The rotor parts are supported via end-plates.

Fig. 3 shows the flowchart exhibiting the selection process for the design parameters and Table 3 shows the radial parameters that were swept in order to maximize the active region torque density. The active region volumetric torque density is defined as

$$T_v = T_3/(\pi r_{o3}^2 d) \tag{4}$$

and the active mass torque density is

$$T_m = T_3/(m_s + m_m) \tag{5}$$

where r_{o3} = outer radius of the MG, d = stack length, m_s = ferromagnetic steel mass and m_m = magnet material mass.

TABLE 1.
STAGE 1 DESIGN REQUIREMENTS

Requirement	Value	Unit
Volumetric torque, T_d	≥250	N·m/L
Efficiency	≥95	%
Torque ripple	≤3	%
Input speed, ω_3	≤ 40	RPM
Rated power	5	kW
Input torque, T_3	≥1193	N·m

TABLE 2.
FIXED STAGE 1 MAGNETIC GEARBOX DESIGN PARAMETERS

Description		Value	Unit
Inner rotor	Pole pair, p_1	6	-
	Steel pole span, θ_1	30	degree
	Airgap, g_i	0.5	mm
Cage rotor	Steel poles, n_2	46	-
	Steel pole span, θ_2	4.22	degree
Outer rotor	Pole pairs, p_3	40	-
	Steel pole span, θ_3	2.25	degree
	Outer radius, r_{o3}	180	mm
	Airgap, g_o	1.5	mm
Axial length, d		40	mm

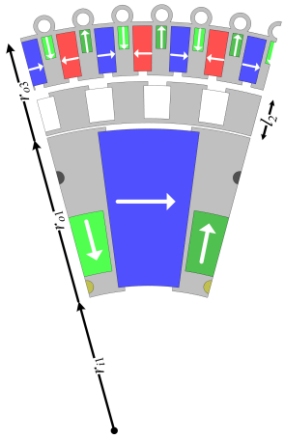

Fig. 3 Geometric variable definitions

The mass and volumetric torque density analysis plot is shown in Fig. 5 for all feasible designs when r_{o3} =180mm. A 2-D JMAG finite element software was used to conduct this analysis. A pareto front is clearly apparent with respect to maximizing mass and volumetric torque density. The r_{o1} =151mm and r_{o1} =148mm parameters give the highest torque density. The torque density values for just these two radii are shown in Fig. 6 and the cage bar length values, l_2, are shown in the legend ($l_2 = r_{o2}$-r_{i2}). By focusing on the r_{o1} = 151mm, a decision can be made based on cage bar length. It can be noted that a larger cage bar length provides better mechanical strength but at the cost of torque density. A cage bar thicknesses greater than l_2 = 13mm starts to significantly impact torque density. The (l_2,r_{o1}) = (12, 151) mm combination was selected as this provided a large radial cage bar thickness whilst also providing a high torque density.

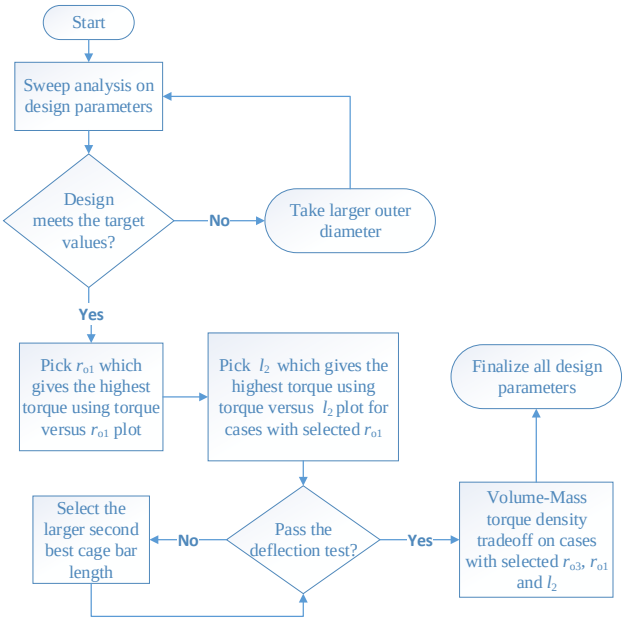

Fig. 4. The flowchart presenting design process

TABLE 3.
VARIED STAGE 1 MAGNETIC GEARBOX DESIGN PARAMETERS

Description		Value [mm]
Inner rotor	Inner radius, r_{i1}	40,42,…,60,65,…95
	Outer radius, r_{o1}	130,133,…,160
Cage rotor	Cage bar length, l_2	9,10,…,15
Outer rotor	Inner radius, r_{i3}	r_{o1}+l_2+g_o+g_i

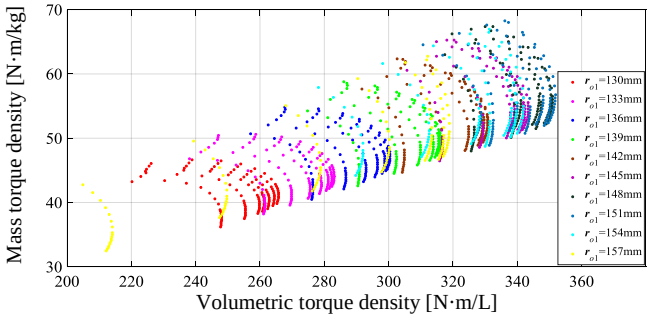

Fig. 5 Active mass torque density and volumetric torque density trade-off analysis for the stage 1 magnetic gearbox.

Fig. 7 shows how the inner rotor inner radius, r_{i1}, impacts volumetric and mass torque density. The volumetric torque density peaks at r_{i1} = 60mm. However, as the mass torque density greatly increases with increased r_{i1} there is little volumetric benefit selected inner radii below r_{i1} = 80mm. It should be noted that this analysis is based on only calculating the active mass torque density and does not account for structural requirements when using a larger inner radius. Fig. 6 shows the final design geometry with (r_{i1},r_{o1},l_2,r_{o3}) = (80,151,12,180) mm parameters. The calculated 2-D FEA torque and torque density is T_3 = 1417N·m and 348N·m/L (for a 40mm axial length).

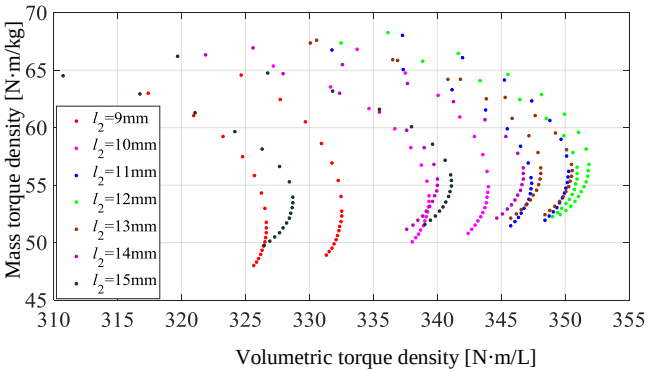

Fig. 6. Active mass torque density and volumetric torque density trade-off analysis for r_{o1} =148mm and r_{o1} = 151mm

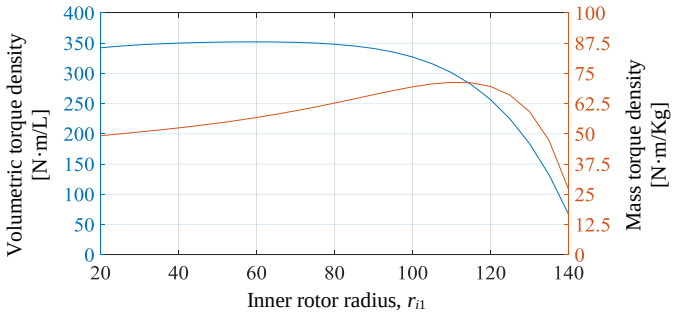

Fig. 5. Stage 1 active mass torque density and volumetric torque density trade-off analysis for varying r_{i1} when (r_{o1},l_2,r_{o3}) = (151mm,12mm,180mm).

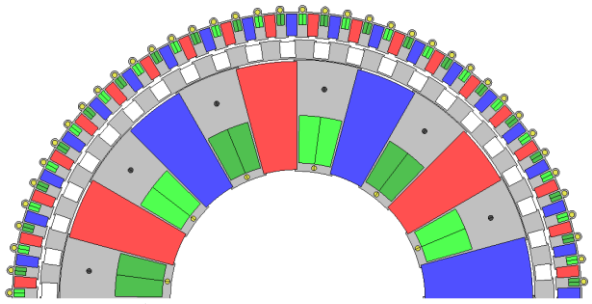

Fig. 6. Final flux concentration stage 1 geometric design when (r_{i1},r_{o1},l_2,r_{o3}) = (80,151,12,180) mm. The 2-D calculated torque density is T_d = 348N·m/L

Fig. 7 shows the torque on the three rotors when the outer rotor and inner rotor are rotating at an angular speed of (ω_3, ω_1) = (40,266.6) RPM (the central cage rotor is fixed). Fig. 8 shows that torque ripple on the outer rotor during a transient decay. It can be noted that a small ripple, less than 1%, is achieved.

A 3-D FEA analysis for the design shown in Fig. 6 was conducted for difference axial lengths. A plot of the percent reduction in torque density between the 2-D and 3-D FEA models as a function of axial length is shown in Fig. 9. At the axial length of d=40mm one can see that the reduction in torque between the 2-D and 3-D model is 27%. An axial length of greater than d = 50mm was deemed to be unacceptable without using additional mechanical support rings. But at d = 50mm the torque reduction is still 24%. As the

plot in Fig. 9 is approximately linear a torque requirement relationship between the 2-D and 3-D models can be defined such that

$$T_{2D} = T_{3D}/[k_e(d)k_s] \quad (6)$$

where $k_e(d)$ is an edge effect reduction function and k_s is an additional safety margin. From Table 2, the required $T_{3D} \geq 1193$. Therefore, with a safety margin of k_s =0.85 and k_e=0.77 the required 2-D torque must be $T_{2D} \geq$ 1815N·m. This 2-D torque value cannot be achieved easily with the flux concentration design and therefore because of this along with outer rotor mechanical deflection concerns an alternative rotor typology was considered.

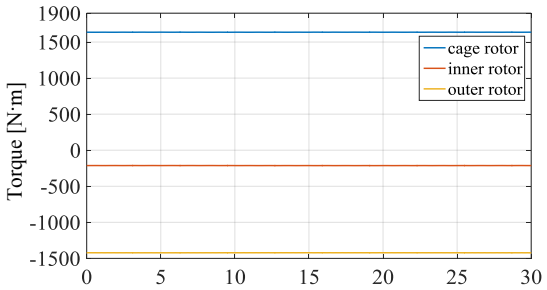

Fig. 7 torque on three rotors

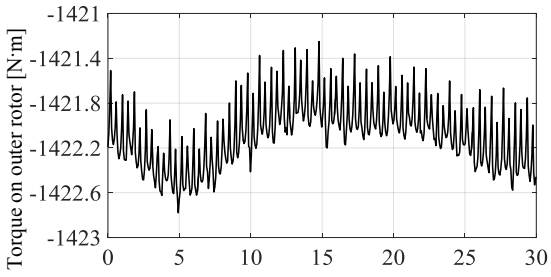

Fig. 8 Torque ripple on outer rotor

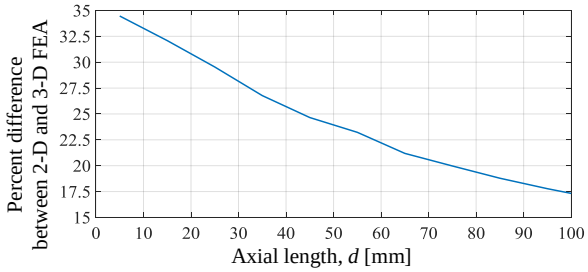

Fig. 9. Plot showing the percent difference between 2-D and 3-D FEA analysis.

B. *Flux Concentration Inner Rotor with Halbach Outer Rotor*

A new outer Halbach rotor approach was investigated for increasing the torque further without increasing the axial length. This typology is shown in Fig. 10. The inner rotor and cage rotor typology were kept the same. In order to make the assembly process easier the outer Halbach rotor back-iron has a slotted design and ferromagnetic steel is used as a back-iron. The use of ferromagnetic material as the back-iron does create a flux leakage path for the Halbach rotor structure, however this was found to not be significant as the field is focused inwards. Fig. 11 compares the field within the back-iron when ferromagnetic and non-ferromagnetic material is used.

To determine the peak torque density for this typology a parametric analysis was again performed where the parameters shown in Table 4 where varied. The resulting analysis is shown in Fig. 12 for two different outer radii r_{o3} = 165 mm and r_o = 170 mm along with a fixed back iron radial length of 25mm. The back-iron length was not taken into account when computing the active region volumetric torque density, using (4), since it is also used as a structural support and helps with assembly.

Fig. 12 shows that the peak volumetric torque density occurs at (r_{o1},l_2) = (142,13). As the r_{o3}=165mm results in the torque value going below the 2-D torque limit of T_{2D}=1815N·m the r_{o3} = 170mm outer radius was selected.

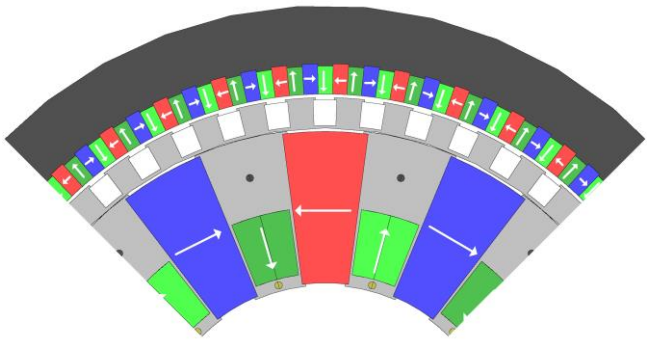
Fig. 10. Quarter view of stage 1 magnetic gear with flux concentration inner rotor and Halbach outer rotor with ferromagnetic back-iron support structure

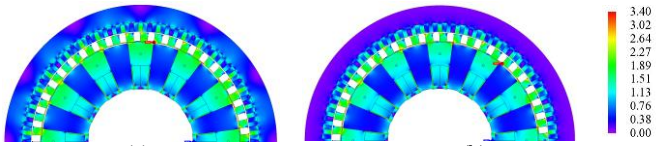

Fig. 11. Magnetic flux density contour plots within back-plate section when (a) back plate made of ferromagnetic and (b) non-ferromagnetic material

TABLE 4.
GEOMETRIC PARAMETERS USED FOR PERFORMANCE ANALYSIS

Design parameter	Symbol	Value [mm]
Inner radius of inner rotor	r_{i1}	50
Outer radius of inner rotor	r_{o1}	120,122,…,144
Cage bar length	l_2	11,12,…,15
MG outer radius	r_{o3}	165, 170
Axial length	d	50
Ferromagnetic back iron radius	r_{o4}	190,195

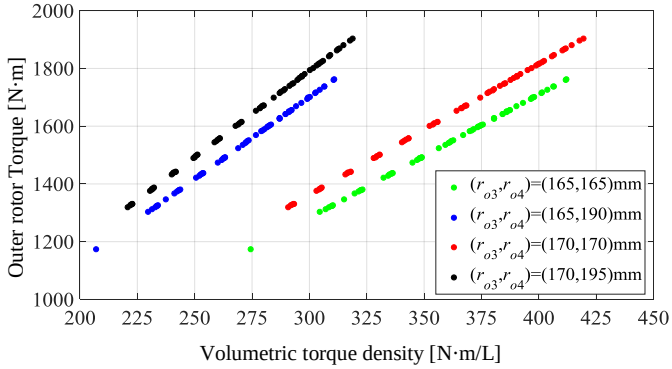

Fig. 12. Torque vs. volumetric torque density for case when r_{o3} = 165 mm and r_{o3} = 170 mm when ferromagnetic back iron is present and not present.

A plot of the volumetric vs. mass torque density when r_{o3} = 170mm is shown in Fig. 13. The plot shows that the maximum volumetric and mass torque density occurs at r_{o1}=142mm. Therefore, this r_{o1} value was picked.

Fig. 14 shows how the torque density changes for different l_2 when (r_{o1}, r_{o3}) = (142, 170)mm. The most important design parameter is the cage bar length as it has a huge impact on both the magnetic field path and mechanical deflection performance. The larger the cage bar length, the more mechanically strong the design. Therefore, in order to avoid deflection, l_2=13mm was selected. This gives a 2-D FEA calculate torque density and torque of T_v = 400N·m/L and T_3 = 1846N·m respectively. This satisfies the 2-D torque requirement ($T_{2D} \geq$ 1815N·m).

The torque as a function of inner radius, r_{i1}, is shown in Fig. 15. Based on the minimum torque value, which satisfies the design target, the r_{i1} =75mm value was selected. Fig. 16 shows the final 3-D MG model and Table 5 summarizes the final geometry parameters.

A 2-D and 3-D transient FEA analysis for the final design was conducted so as to re-check the torque and torque ripple. Fig. 18 shows the calculated torque on the three rotors when the angular rotor speeds are (ω_1, ω_3) = (40, 266.6) RPM. The reduction in torque between the 2-D and 3-D models is apparent. The peak 3-D FEA calculated torque is T_3 = 1391 N·m, which corresponds to a volumetric and mass torque density of T_d = 306.4 N·m/L and T_m= 56.2 N·m/kg respectively. Fig. 18 shows the torque ripple on the outer rotor a torque ripple of less than 1% was achieved at peak torque.

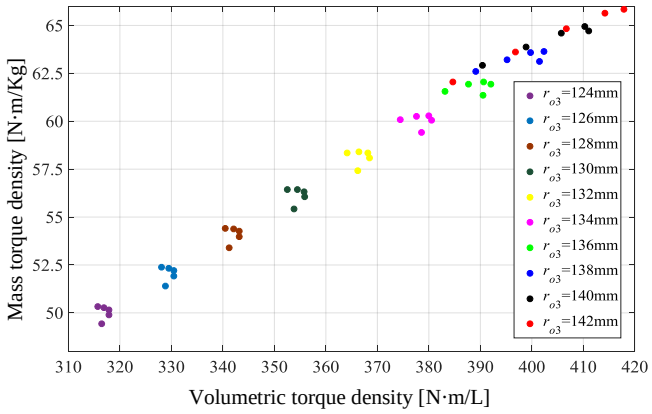

Fig. 13. Active mass torque density and volumetric torque density trade-off analysis for r_{o3} = 170 mm.

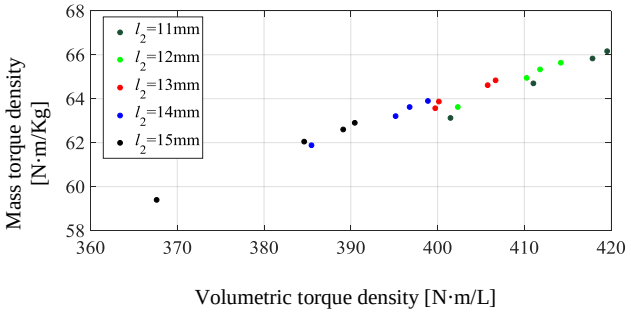

Fig. 14. Active mass torque density and volumetric torque density trade-off analysis for (r_{o1}, r_{o3})=(142, 170)mm

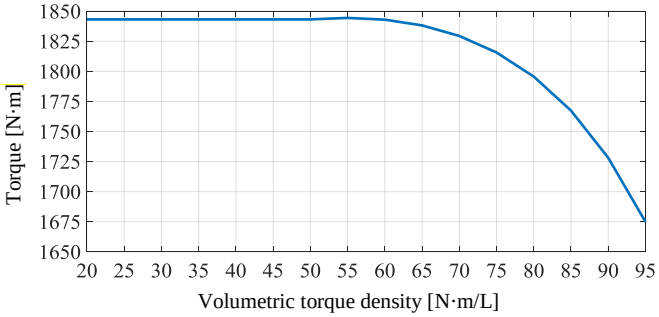

Fig. 15. Torque vs. r_{i1} for (r_{o1}, l_2, r_{o3})=(142,13,170) mm

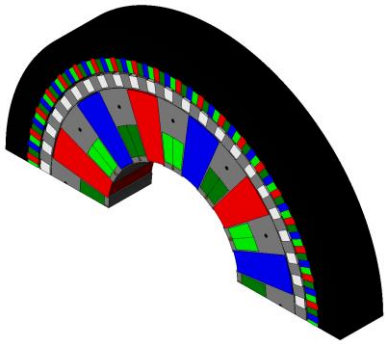

Fig. 16. A 3-D model of the MG with slotted outer rotor back iron

TABLE 5.
FINAL DESIGN PARAMETERS

Description		Value	Unit
Inner rotor	Pole pair, p_1	6	-
	Steel pole span, θ_1	30	degree
	Airgap, g_i	0.5	mm
	Radial length	67	mm
Cage rotor	Steel poles, n_2	46	-
	Steel pole span, θ_2	4.07	degree
	Radial length	13	mm
Outer rotor	Pole pairs, p_3	40	-
	Steel pole span, θ_3	2.25	degree
	Outer radius, r_{o3}	170	mm
	Airgap, g_o	1.5	mm
	Radial length	13	mm
	Back iron radius, r_{o4}	195	mm
Axial length, d		50	mm

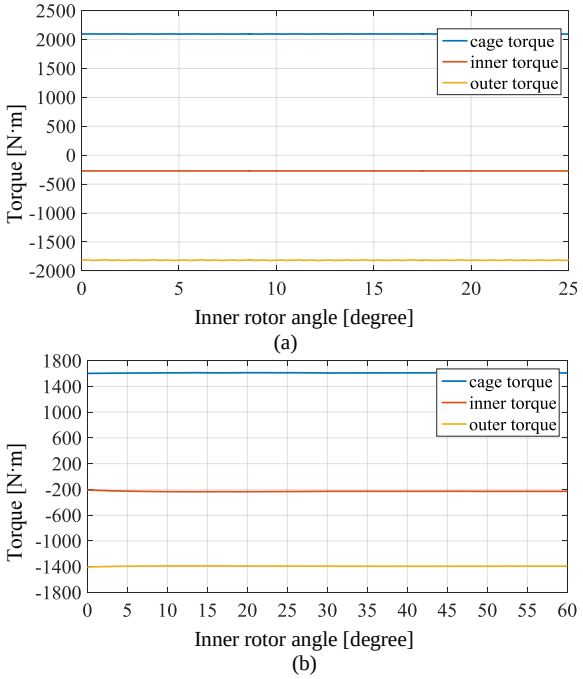

Fig. 17.(a) 2-D transient FEA calculated torque and (b) 3-D transient FEA calculated torque on all three rotors

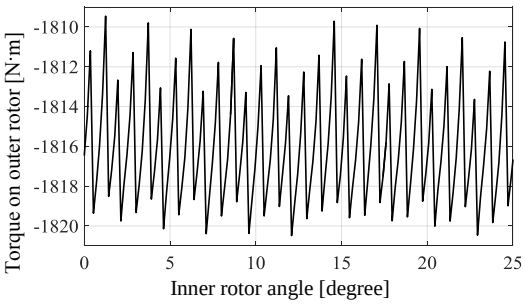

Fig. 18. (a) Torque ripple on the outer rotor at peak condition.

The power relation between the MG rotors is

$$|T_1|\omega_1 - |T_3|\omega_3 = P_l \qquad (7)$$

where P_l are the total MG loss. The losses can be separated such that

$$P_l = P_h + P_e + P_m \qquad (8)$$

where P_h = hysteresis losses, P_e = eddy current losses, P_m = mechanical losses (primarily due to bearings and windage). The efficiency can then be computed from

$$\eta = \frac{|T_1|}{|T_3|} \cdot G_r \qquad (9)$$

Using the 3-D FEA analysis the efficiency and power loss at ω_1= 40RPM was computed to be 91% when the back-iron is not laminated. However, when the back-iron is laminated the calculated efficiency increased to 98% indicating that while the Halbach array focuses the field inwards a sizable amount of time-changing field does pass through into the back-iron. Table 6 provides a comparative summary of the calculated final values and the specified values.

TABLE 6.
TORQUE DENSITY PERFORMANCE FOR FINAL DESIGN

Metric		2-D FEA	3-D FEA	Specified	Units
Input torque, T_3		1815	1391	≥1193	N·m
Torque density	Volumetric, T_d	399.9	306.4	≥250	N·m/L
	Magnet mass, T_m	113.7	87.1		N·m/kg
	Mass, T_m	74.2	56.2		N·m/kg
Efficiency		-	98	≥ 95	%
Torque ripple		-	1	≤3	%

IV. MECHANICAL DEFLECTION ANALYSIS

A mechanical deflection analysis was performed to ensure that the components do not significantly deflect relative to the airgap length. For the inner and cage rotor, the support rods are assumed to endure all the forces. The 2-D FEA calculated radial and tangential force values at different radial positions for the inner rotor and cage rotor support elements are shown in Fig. 19 and Fig. 20.

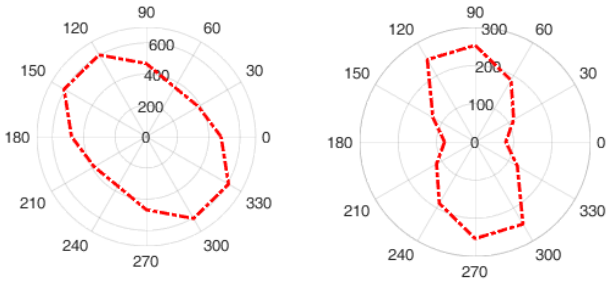

(a) (b)

Fig. 19. (a) Radial and (b) tangential force (N) at difference radial positions for the inner rotor elements

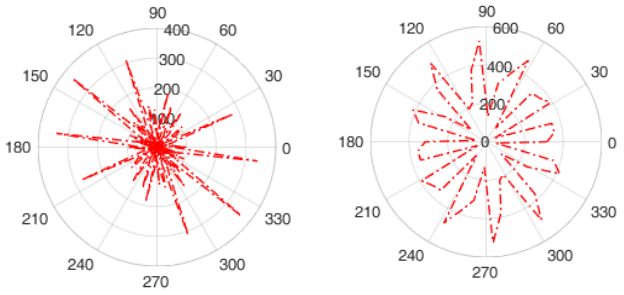

Fig. 20. (a) Radial and (b) tangential force (N) at difference radial positions for the cage rotor elements

Using the force values given in Fig. 19 a 3-D FEA mechanical deflection analysis was conducted using ANSYS on the inner rotor laminations. Fig. 21(a) shows the computed deflection when the scaled force was applied to the support rod and one lamination, while Fig. 21(b) shows the resultant deflection when including the force on each of the laminations. The deflection on the two rods is amplified in the plots. In Fig. 21(a) a peak deflection of 0.116mm (23% of air-gap) was calculated while using the model shown in Fig. 21(b) the deflection was only 0.0039mm, or 0.8% of the airgap.

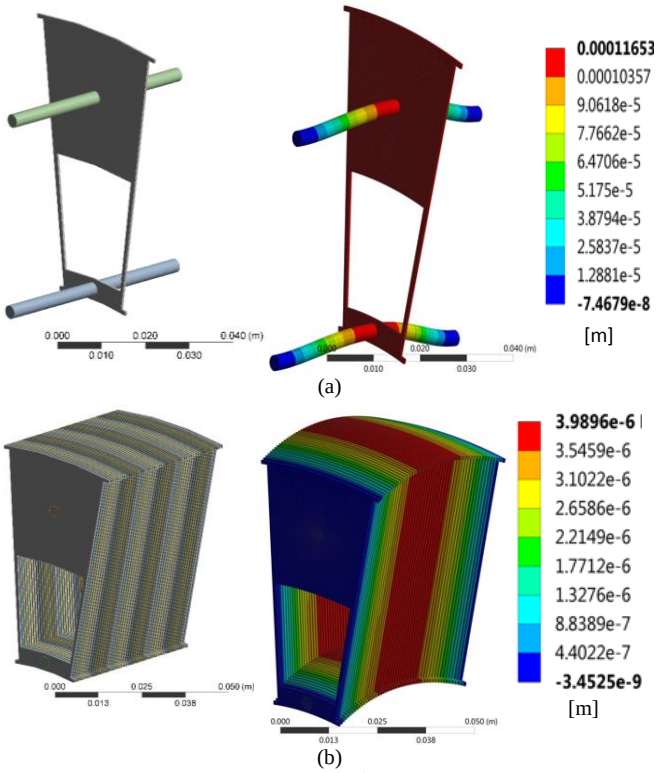

Fig. 21. Finite element analysis deflection analysis on the inner rotor when (a) not accounting for laminated stack effect and (b) when including laminated effect

The cage rotor deflection was also investigated. Using the force values shown in Fig. 20 the deflection on the cage rotor was calculated for the case when the cage rotor laminations are supported using Garolite G10 bars. Fig. 22 shows support bars deflection in the absence of lamination effect (One lamination in the middle is there for the unity of the bars passing through cage laminations). The maximum deflection is 0.0162mm which is considerably smaller than the gap (0.5mm). Knowing that Garolite bars are supported

by lamination's small teeth, deflection analysis on teeth area was also performed. As shown in Fig. 23 a maximum deflection in the lamination teeth area is calculated to be 0.00119mm which is a very small deflection Therefore, based on this mechanical analysis the mechanical design is expected to be robust.

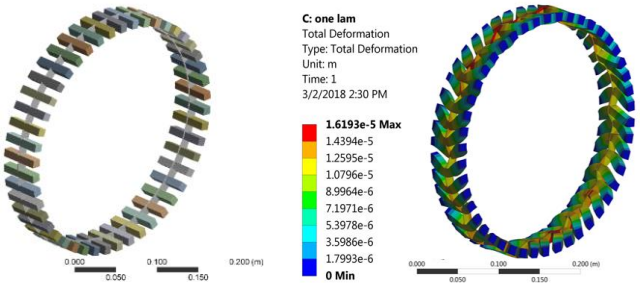

Fig. 22.Support bars deflection in the absence of lamination effect (One lamination in the middle is there for the unity of the bars passing through cage laminations)

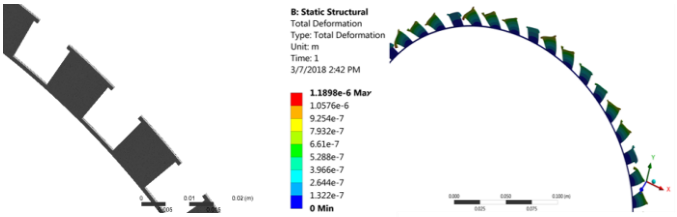

Fig. 23. Maximum deflection in lamination teeth area

V. Conclusion

This paper presented a electromagnetic as well as mechanical deflection analysis of a new type of rotary MG typology for a hermetically sealed multistage MGG. A mass and volumetric torque density analysis was conducted combined with a 3-D FEA analysis. A flux focusing inner rotor and Halbach outer rotor typology was selected as it was calculated to be able to achieve the necessary torque and torque density without using an excessive axial length. Currently the presented MG is being fabricated.

Acknowledgment

The authors would gratefully like to thank the JMAG Corporation for the use of their FEA software. This material is based upon work supported by the Department of Energy under grant number DE-EE0008100.

References

[1] S. Benelghali, M. E. H. Benbouzid, and J. F. Charpentier, "Generator systems for marine current turbine applications: a comparative study," *IEEE Jour. Oceanic Eng.* , vol. 37, no. 3, July 2012.

[2] W. Musial, S. Butterfield, and B. McNiff, "Improving Wind Turbine Gearbox Reliability," National Renewable Energy Laboratory, NREL/CP-500-41548, May 2007.

[3] M. A. Mueller, H. Polinder, and N. Baker, "Current and novel electrical generator technology for wave energy converters," in *IEEE Elect. Mach. Dri. Conf.*, Antalya, Turkey, pp. 1401 - 1406, 3-5 May, 2007.

[4] T. J. E. Miller, *Brushless Permanent-Magnet and Reluctance Motor Drives*: Oxford University Press, 1989.

[5] M. Johnson, M. C. Gardner, H. A. Toliyat, S. Englebretson, W. Ouyang, and C. Tschida, "Design, construction, and analysis of a large scale inner stator radial flux magnetically geared generator for wave energy conversion," presented at the *IEEE Energy Conv. Cong. Expo.*, Cincinnati, OH, 1-5 Oct., 2017.

[6] L. Shah, A. Cruden, and B. W. Williams, "A variable speed magnetic gear box using contra-rotating input shafts," *IEEE Trans. Mag.*, vol. 47, no. 2, pp. 431-438, 2011.

[7] J. Bird, "Marine hydrokinetic power take-off using magnetic gearing," presented at the *2nd Marine Energy Technology Symposium*, Seattle, WA, April 15-18, 2014.

[8] B. McGilton, M. Mueller, and A. McDonald, "Review of magnetic gear technologies and their applications in marine energy," in *5th IET Intern. Conf. Renew. Power Gen.*, London, UK, pp. 1-6,21-23 Sept. 2016.

[9] K. Atallah, S. D. Calverley, and D. Howe, "Design, analysis and realisation of a high-performance magnetic gear," *IEE Proc.-Electr. Power Appl.*, vol. 151, no. 2, pp. 135-143, 2004.

[10] K. K. Uppalapati, J. Z. Bird, J. Wright, J. Pitchard, M. Calvin, and W. Williams, "A magnetic gearbox with an active region torque density of 239N·m/L," *IEEE Trans. Ind. Appl.*, Vo. 54, No.2, pp. 1331 - 1338, 2018.

[11] T. V. Frandsen, L. Mathe, N. I. Berg, R. K. Holm, T. N. Matzen, P. O. Rasmussen, *et al.*, "Motor integrated permanent magnet gear in a battery electrical vehicle," in *IEEE 2013 Energy Conv. Cong. Expo.*, Denver, CO, pp. 2170-2177,Sept. 15-19, 2013.

[12] K. Atallah, J. Rens, S. Mezani, and D. Howe, "A novel "pseudo" direct-drive brushless permanent magnet machine," *IEEE Trans. Magn.* , vol. 44, no. 11, pp. 4349–4352, Nov. 2008.

[13] B. D. Hibbs and B. X. Phan, "Flux Concentrator for ironless motors," USA Patent Application, 20100181858 A1, Jul. 22 ,2010.

[14] D. Som, K. Li, J. Kadel, J. Wright, S. Modaresahmadi, J. Z. Bird, *et al.*, "Analysis and Testing of a Coaxial Magnetic Gearbox With Flux Concentration Halbach Rotors," *IEEE Trans. on Magn.*, vol. 53, no. 11, pp. 1-6, 2017.